Temperature Dependent Charge Carrier Dynamics in Formamidinium Lead Iodide Perovskite

Gélvez-Rueda, María C.; Renaud, Nicolas; Grozema, Ferdinand C.

DOI
10.1021/acs.jpcc.7b09303

Publication date
2017

Document Version
Final published version

Published in
The Journal of Physical Chemistry C

Citation (APA)
Gélvez-Rueda, M. C., Renaud, N., & Grozema, F. C. (2017). Temperature Dependent Charge Carrier Dynamics in Formamidinium Lead Iodide Perovskite. *The Journal of Physical Chemistry C*, *121*(42), 23392-23397. https://doi.org/10.1021/acs.jpcc.7b09303

Important note
To cite this publication, please use the final published version (if applicable).
Please check the document version above.

THE JOURNAL OF PHYSICAL CHEMISTRY C

Article

Cite This: J. Phys. Chem. C 2017, 121, 23392-23397

pubs.acs.org/JPCC

Temperature Dependent Charge Carrier Dynamics in Formamidinium Lead Iodide Perovskite

María C. Gélvez-Rueda, Nicolas Renaud, and Ferdinand C. Grozema*

Optoelectronic Materials Section, Department of Chemical Engineering, Delft University of Technology, Van der Maasweg 9, 2629 HZ, Delft, The Netherlands

Supporting Information

ABSTRACT: The fundamental opto-electronic properties of organic−inorganic hybrid perovskites are strongly affected by their structural parameters. These parameters are particularly critical in formamidinium lead iodide ($FAPbI_3$), in which its large structural disorder leads to a non-perovskite yellow phase that hinders its photovoltaic performance. A clear understanding of how the structural parameters affect the opto-electronic properties is currently lacking. We have studied the opto-electronic properties of $FAPbI_3$ using microwave conductivity measurements. We find that the mobility of $FAPbI_3$ increases at low temperature following a phonon scattering behavior. Unlike methylammonium lead iodide ($MAPbI_3$), there are no abrupt changes after the low-temperature β/γ phase transition and the lifetime is remarkably long. This absence of abrupt changes can be understood in terms of the reduced rotational freedom and smaller dipole moment of the formamidinium, as compared to methylammonium.

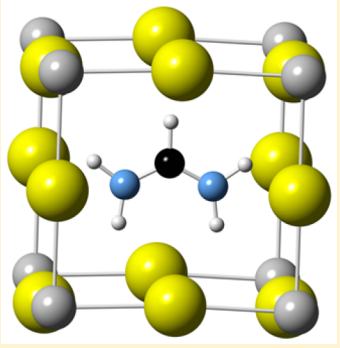

INTRODUCTION

The opto-electronic properties of organic−inorganic metal halide perovskites strongly depend on their composition and the degrees of freedom within the structure.[1,2] Interactions related to the motion of the organic cation, soft rotation of the inorganic octahedra, and the stereochemistry of Pb^{2+} have been shown to affect properties such as the mobility of charges,[3−5] charge carrier lifetime,[3−5] band gap,[6−9] geometry of the unit cell,[10] and dimensionality of the crystal structure.[7,10−14] The latter effect is critical in formamidinium lead iodide ($FAPbI_3$) as it can lead to the formation of a non-perovskite yellow phase that hinders its photovoltaic performance.[10,15] Replacing methylammonium (MA) by formamidinium (FA) appears a straightforward alternative as it leads to a decrease in the band gap of $FAPbI_3$ to 1.47 eV and therefore an improvement in the absorption in the infrared region.[15−20] However, the formation of the non-perovskite yellow phase decreases the stability and solar cell efficiency and complicates the understanding of its intrinsic opto-electronic properties.[21,22] Studies to clarify the intrinsic opto-electronic properties of $FAPbI_3$ are limited. Photoluminescent measurements at room temperature have shown that the diffusion length of the charge carriers is considerably longer in $FAPbX_3$ than in $MAPbX_3$ (X = I, Br) perovskites.[19,20,23−25] Furthermore, based on a line-width analysis of photoluminescence measurements, it has been argued that charge transport is dominated by scattering from optical phonons (Fröhlich interactions) instead of acoustic phonons as has been assumed ealier for $MAPbX_3$.[26] Currently, there are no studies that focus on properties such as charge mobility and recombination mechanisms as a function of temperature. Moreover, no studies have been reported that relate changes in these properties to the presence of the organic cation within the perovskite structure.

The reorganization of the organic cation in the perovskite lattice of $MAPbI_3$ has a large influence on the crystal phase geometry,[10] the charge carrier dynamics (mobility and recombination mechanisms),[3−5] and the optical-electronic transitions (direct−indirect band gap[8,9], Rashba splitting[9]). Replacing MA by FA should affect the reorientation of the organic cation due to the larger size and smaller dipole moment of FA. Indeed, it has been calculated that the time constant for the rotation of FA is 1 order of magnitude longer than that for MA.[27,28] This is consistent with the larger size of FA, which reduces its rotational freedom in the structure. In addition, temperature dependent dielectric measurements show that, compared to $MAPbI_3$, the static dielectric permittivity (ε_r') of $FAPbI_3$ is lower and has a negligible temperature dependence.[29−31] This is consistent with the smaller dipole moment of FA.[31] Moreover, at temperatures below the tetragonal (β) to orthorhombic (γ) phase transition, the ε_r' of $FAPbI_3$ continues increasing while in $MAPbI_3$ abruptly decreases.[29−31] This means that the rotational freedom of FA is maintained and is less affected by temperature than the rotational freedom of MA, which is drastically reduced at low temperatures.[31] We have shown recently that, in the low-temperature orthorhombic phase of $MAPbI_3$, where the MA orientation is static, the charge carrier mobility and lifetime abruptly increase.[5] This behavior is attributed to the formation of polar charged domains that increase charge separation and reduce recombination.[3−5] In this

Received: September 19, 2017
Revised: September 29, 2017
Published: October 2, 2017

DOI: 10.1021/acs.jpcc.7b09303
J. Phys. Chem. C 2017, 121, 23392−23397

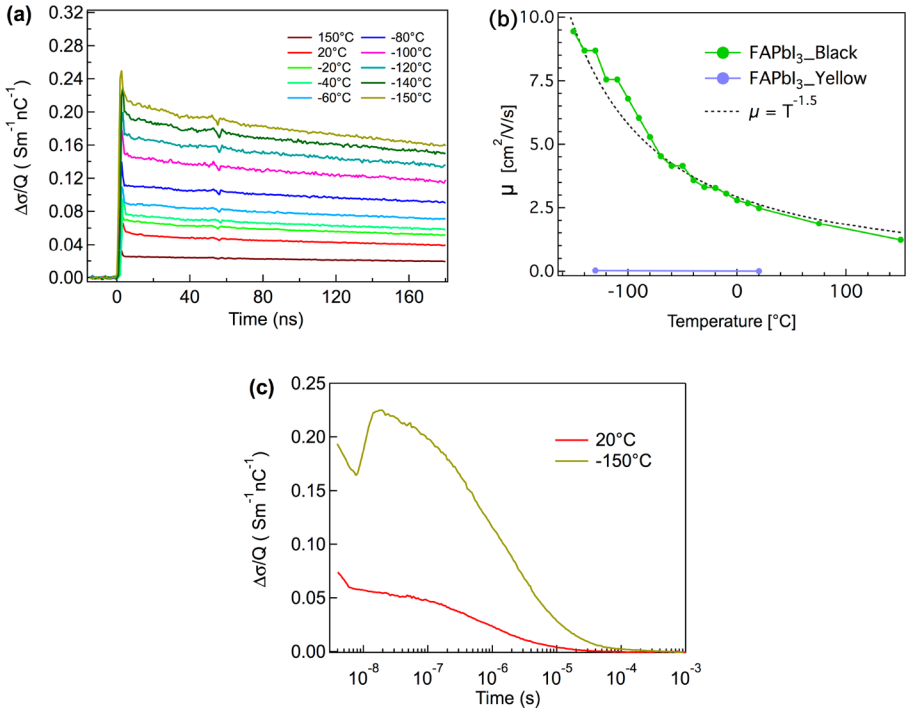

Figure 1. Radiation induced conductivity for the black $FAPbI_3$ material as a function of time using a 0.2 ns electron pulse (a), charge carrier mobility as a function of temperature (b), and long-time decay of the carrier lifetime (c).

work, we have studied the temperature dependence of the mobility and lifetime of charge carriers in $FAPbI_3$ using time-resolved microwave conductivity measurements, coupled with generation of charges by irradiation with high-energy electrons (PR-TRMC). We show that the charge carriers mobility of $FAPbI_3$ increases at low temperature following phonon scattering behavior ($\mu \sim T^{-1.5}$). Interestingly, in contrast to our previous results for $MAPbI_3$,[5] we do not observe sudden changes in the mobility and lifetime of charge carriers at temperatures below the β/γ phase transition. We attribute this to the persisting rotational freedom of FA in the orthorhombic phase. As FA does not become fixed in the structure, it does not form charged domains that suddenly increase the mobility and lifetime at the phase transition. The much smaller dependence of the orientational freedom of FA on temperature is primarily related to the smaller dipole moment of FA, compared to MA. This work confirms that the charge carrier dynamics in hybrid perovskites are affected by the intrinsic properties of the organic cation and its interaction within the structure.

EXPERIMENTAL SECTION

Starting Materials. All chemicals were purchased from Sigma-Aldrich and used as received. Formamidinium iodide (FAI) was synthesized by neutralizing equimolar amounts of 57 wt % aqueous hydriodic acid (HI) and 99 wt % formamidine acetate salt ($HN{=}CHNH_2{\cdot}CH_3COOH$) at 0 °C for 1 h. The white precipitate was collected by evaporation of the solvent using rotary evaporation at 50 °C under reduced pressure. The precipitate was washed three times with diethyl ether by pump air filtration, recrystallized in ethanol, and dried under vacuum for 24 h before use.

$FAPbI_3$ Synthesis. The precursors $HC(NH_2)_2I$ and PbI_2 (99.999%) were mixed at a molar ratio of 1.5:1 and dissolved in anhydrous DMF at varying dilution rates (40, 20, 10 wt %, 0.88 M). This molar ratio was used in order to obtain pure perovskites phases. The solutions were ultrasonically stirred for 15−30 min to ensure complete dissolution. The resulting precursor solution was placed in a vacuum oven at 10^{-2} mbar and heated in steps of 10 °C every 20 min up to 130−140 °C. After the maximum temperature was reached, the samples were left 30 min in the vacuum oven in order to ensure the complete evaporation of the solvent and annealing of the perovskite crystals. Higher temperatures are undesirable as this induces thermal degradation. The 0.88 M dilution assured the synthesis of the $FAPbI_3$ black phase. This polycrystalline phase is stable in dry air but interconverts to the yellow phase in a couple of weeks. The black phase can be recovered heating the crystals to 140 °C for 30 min.

Preparation of PR-TRMC Sample Holders. A small amount of $FAPbI_3$ (~40 mg) is placed in a polyether ether ketone (PEEK) holder and covered by poly(methyl methacrylate) (PMMA) dissolved in chlorobenzene (10 mg/mL). The PMMA layer protects the samples from the environment and diminishes the background conductivity (which affects the PR-TRMC measurements).

PR-TRMC Measurements. In the PR-TRMC setup, the sample holder is placed in a microwave cell. Subsequently, the microwave cell is placed in a cryostat where the temperature can be varied between −150 and 200 °C. The temperature is maintained for ~15 min before every measurement to ensure the equilibrium of the system. The irradiation intensity was varied between pulse lengths of 200 ps and 1 ns for each temperature at a frequency of 32 GHz. The frequency scan (28−38 GHz) fits were measured at a pulse length of 200 ps.

DFT Calculations. All DFT calculations were performed with the BAND program included in the Amsterdam Density Functional suite. During the calculation, the experimental geometry was used. The electronic structure calculations were performed using a triple-ζ basis set (TZP) and without using frozen cores. The PBEsol functional was used to account for

DOI: 10.1021/acs.jpcc.7b09303
J. Phys. Chem. C 2017, 121, 23392−23397

exchange and correlation. Relativistic effects were included via a scalar correction of the ZORA. The effective masses were calculated using the internal capabilities of BAND.

RESULTS AND DISCUSSION

We prepared micrometer crystals of $FAPbI_3$ from an anhydrous DMF solution (0.88 M) by evaporation of the solvent under reduced pressure (10^{-2} mbar). We optimized the synthesis conditions in order to isolate black α-$FAPbI_3$ (see XRD in Figure S1). The black α-$FAPbI_3$ phase was obtained and stabilized at higher temperature (160 °C for at least 1 h) in comparison to the yellow phase (140 °C). This procedure is in agreement with the literature, where the black phase is stabilized at 185 °C for 1 h under ambient pressure conditions.[23,25] The black α-$FAPbI_3$ crystals remain in this phase at room temperature for 7−15 days before converting to the yellow phase. The crystals were placed in a polyimide container and sealed with a PMMA layer deposited from a 10 mg/mL solution in chlorobenzene to avoid degradation.

The charge carrier mobility and charge recombination mechanisms were studied by Pulse-Radiolysis Time-Resolved Microwave Conductivity (PR-TRMC) experiments. In this technique, charge carriers are generated by irradiating the sample with a short pulse of high-energy electrons (3 MeV). If the free charge carriers generated in this way are mobile, this results in a fractional absorption of microwave power reflected by the cell that is directly proportional to the change in conductivity of the material studied (eq 1)

$$\frac{\Delta P}{P} = A\Delta\sigma \tag{1}$$

where P is the incident microwave power, $\Delta\sigma$ is the change in conductivity on generation of charges, and A is a sensitivity factor that is dependent on the geometry of the measurements cells and the dielectric properties of the sample.

The use of a short pulse of high energy electrons to generate charge carriers has several advantages over photogeneration of charges. First of all, electron−hole pairs are generated with a large distance between the opposite charges, larger than the Coulomb radius. Second, the electron−hole pairs are generated at a relatively low concentration with a uniform profile throughout the material. This differs from generation by laser excitation, such as that used in PL and tera-Hertz spectroscopy, where opposite charge carriers are generated close to each other with a rather steep concentration gradient. These differences are critical for temperature dependent measurements, since, at low temperatures, charge carriers generated by photoexcitation cannot dissociate due to the formation of a bound exciton.[24] Using high-energy electrons, we can determine the temperature dependence of the conductivity and charge carrier mobility independent of the excitation wavelength and exciton binding energy of the material studied.

Typical conductivity transients for black $FAPbI_3$ as a function of temperature are shown in Figure 1a. The conductivity increases during the pulse as mobile charge carriers are generated, and subsequently decreases as the charge carriers recombine or become trapped. In Figure 1a, it is seen that, for black $FAPbI_3$, the change in conductivity at the end of the pulse increases as the temperature decreases. We estimate the mobility knowing the initial concentration of charge carriers at the end of the electron pulse ($N_p(0)$) according to eq 2. $N_p(0)$ is a function of the irradiation energy deposited per unit volume of the sample. The mobility determined (μ) is the sum of the mobilities for electrons and holes and is shown in Figure 1b. A more detailed description of this technique can be found in previous studies.[5,32−34]

$$\Delta\sigma = e\sum N_p(0)\mu = e(n_n\mu_n + n_p\mu_p) \tag{2}$$

We determined that the charge carrier mobility of black $FAPbI_3$ is ∼2.5 $cm^2/(V{\cdot}s)$ at room temperature (Figure 1b). This value is lower than that determined for thin films by tera-Hertz (∼27 $cm^2/(V{\cdot}s)$) but comparable to values derived on the basis of photoluminesce experiments (μ_h = 3.5 $cm^2/(V{\cdot}s)$ and μ_e = 0.2 $cm^2/(V{\cdot}s)$).[35] For single crystals, Space-Charge-Limited Current (SCLC) experiments have also resulted in a higher charge mobility (μ_h = 35 $cm^2/(V{\cdot}s)$).[35] The lower value that we obtain here may be related to the polycrystalline nature of our crystals (see Figure S2 in the Supporting Information (SI)). In addition, we observe that the charge carrier mobility increases as the temperature decreases, up to ∼9.5 $cm^2/(V{\cdot}s)$ at −150 °C. As a comparison, we show that the charge carrier mobility of black $FAPbI_3$ is 2 orders of magnitude higher than that for the yellow $FAPbI_3$ (0.009 $cm^2/(V{\cdot}s)$ at 20 °C). This is fully consistent with DFT calculations that show that the effective masses of electrons and holes in the yellow phase are 3−10 times higher than those in the black phase (Table S1 in the SI). The increase of the charge carrier mobility of black $FAPbI_3$ with decreasing temperature follows the acoustic phonon−electron scattering (lattice vibration) trend of classic semiconductors such as silicon ($\mu \sim T^{-1.5}$) at all the temperatures measured.[36] Interestingly, in contrast to previous work on $MAPbI_3$,[5] we do not observe a deviation from this phonon-scattering trend at temperatures below the tetragonal (β) to trigonal (γ) phase transition (−133 °C[30,31]).

We have also studied the charge carrier lifetime of $FAPbI_3$ as a function of temperature. In Figure 1a, we observe that, even at room temperature, the carrier lifetime of $FAPbI_3$ is long and does not significantly decay in the first 200 ns. In Figure 1c, the conductivity decay is shown on a logarithmic time scale, where it can be seen that the carrier lifetime increases from ∼600 ns at room temperature to over 2 μs at −150 °C. These lifetimes can be compared to carrier life times obtained from photoluminescence measurements that have been shown to give lifetimes ranging between 100 and 600 ns at room temperature for $FAPbI_3$, depending on the preparation method of the sample.[23−25] We fit the decay and use the charge carrier mobility determined to estimate a carrier diffusion length of ∼1 μm. This value is comparable to that of $FAPbI_3$ polycrystalline thin films (3.1 μm)[20,24] and single crystals (6.6 μm).[23,25] We made the same analysis for similar samples of $MAPbI_3$, determining a carrier diffusion length of ∼0.6 μm (see Figure S3 in the SI). Similar to previous photoluminescence studies, we find that, at room temperature, the carrier lifetime of $FAPbI_3$ is longer than that in $MAPbI_3$.[19,20,23−25] We believe that the longer carrier lifetime of $FAPbI_3$ is caused by the reduced rotational freedom of FA as compared with MA. It has been shown, both experimentally and theoretically, that the time for the rotation of MA is ∼0.3 ps for a wobbling-in-a-cone motion and ∼3 ps for 90° jumps.[27] In the case of FA, the theoretical rotation is ∼2 ps for the rollover process.[28] This slower rotation leads to polar rotations and distorted domains that also distort the inorganic cages, ultimately facilitating charge separation and reducing recombination.[25] In addition, we do not observe an abrupt increase of the carrier lifetime of $FAPbI_3$ at temperatures below the β/γ phase transition. In fact,

DOI: 10.1021/acs.jpcc.7b09303
J. Phys. Chem. C 2017, 121, 23392−23397

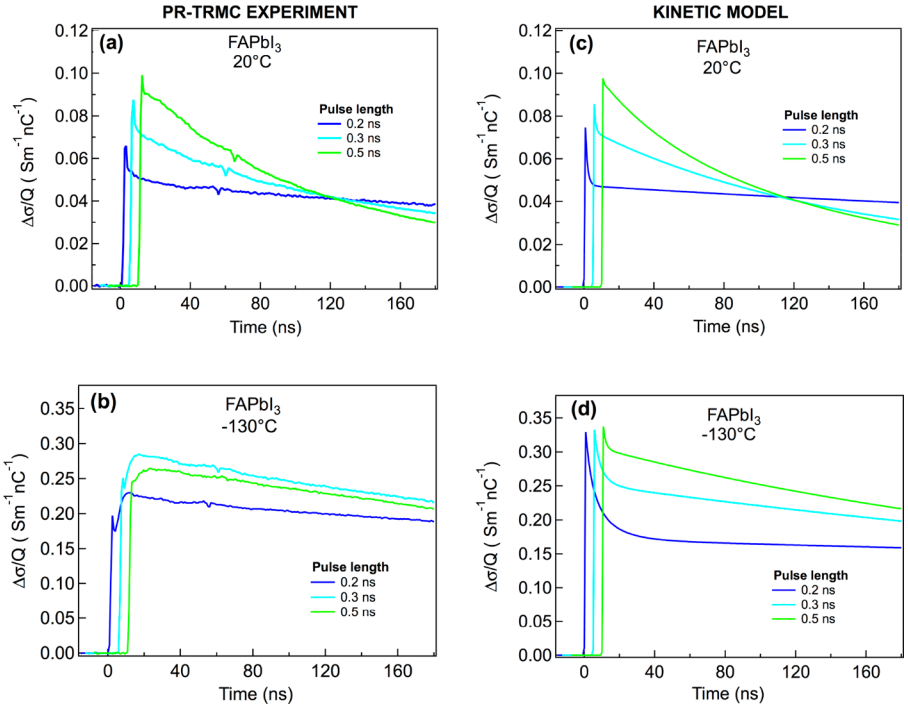

Figure 2. Experimental (a, b) and kinetic model fit (c, d) pulse length dependence of $FAPbI_3$ at room and low temperature.

the increase of the carrier lifetime of $FAPbI_3$ at low temperature is not large. The standard deviation of the time constants, obtained by fitting the decay, is only of 47 ns over the whole temperature range (see Figure S4 in the SI). These results confirm that, at temperatures below the γ phase transition, neither the charge carrier mobility nor lifetime of $FAPbI_3$ abruptly increase as it occurs for $MAPbI_3$.

For hybrid perovskites ($MAPbI_3$ and $FAPbI_3$), the dependence of the charge carrier dynamics on temperature have been mainly related to phonon scattering mechanisms dominated by interactions between charge carriers and optical phonons (Fröhlich interactions).[26,37] However, the influence of only Fröhlich interactions does not explain the low charge carrier mobility of hybrid perovskites (compared to inorganic semiconductors with similar Fröhlich coupling strengths),[26,38] neither the abrupt increase of the charge carrier mobility and lifetime of $MAPbI_3$ at temperatures below the tetragonal (β) to orthorhombic (γ) phase transition.[5,38] This latter effect has been related to the fixed orientation of MA in the γ phase,[29,39,40] which leads to strong polar domains that increase charge separation and reduce recombination.[3−5] In the case of $FAPbI_3$, the mobility and lifetime of $FAPbI_3$ do not abruptly increase in the γ phase. This is consistent with the persistent reorientation of FA in the γ phase observed by dielectric experiments.[31] The static dielectric permittivity (ε_r'), which indirectly probes the motion of the organic cation, does not decrease on going through the β/γ phase transition and continues increasing in the γ phase.[31] The reorientation of FA is mildly inhibited at these temperatures.[31] The low ε_r' and its minimal dependence on the temperature are consistent with the small dipole moment of FA.[31] This behavior is completely opposite to $MAPbI_3$, in which the ε_r' abruptly decreases due to the reduced rotational freedom of MA on going through the β/γ phase transition.[29] Comparing the present experiments on $FAPbI_3$, with our previous work on $MAPbI_3$, we have clearly shown that the charge carrier dynamics are strongly dependent on the nature of the organic cation. We believe that the vibrational mechanisms are affected by the organic cation rotation (dipole scattering) within the structure.[5,38] This interaction strongly depends on the intrinsic properties of the organic cation, such as size and strength of dipole moment.

In addition, with PR-TRMC, it is possible to vary the initial concentration of charges (varying the length of the electron pulse) to obtain information about trapping, recombination processes, and carrier lifetimes from the temporal decay of the conductivity. In Figure 2a,b, we show the experimental conductivity as a function of time at 20 and −130 °C, varying the pulse length between 0.2 and 0.5 ns. This results in initial concentrations between 6×10^{14} and 3×10^{15} cm^{-3}. This generation rate is lower than with a 1.5 AM solar simulator (10^{16} cm^{-3}).[41,42] Nevertheless, it allows us to study the dynamics at conditions that are not feasible with a laser-TRMC or THz experiments (10^{16}−10^{18} cm^{-3}). In Figure 2a,b, we observe that the conductivity at the end of the pulse increases with the initial concentration, while the lifetime becomes shorter. This behavior is similar to that previously reported for $MAPbX_3$ (X = I, Br).[5] In our previous work,[5] we proposed that the dynamics can be explained by second-order recombination with the presence of a limited concentration of trap states for either the electron of the hole. We use the same kinetic model for the decay of charge carriers to determine the trap concentration, rate of recombination of each process, and mobility (Table 1).[5]

In Figure 2c,d, it is seen that the kinetic model reproduces the main features of the conductivity as a function of temperature. In general, the results of the fits are similar as for $MAPbI_3$.[5] The mobility of the individual charges (electrons/holes) determined by our fits are similar to the electron mobility being slightly higher. This is in agreement with our DFT band structure calculations (Table S1 in the SI). In this analysis, we assumed that the electrons become trapped;[15,43] however, the nature of the traps is not known. The

DOI: 10.1021/acs.jpcc.7b09303
J. Phys. Chem. C 2017, 121, 23392−23397

Table 1. Kinetic Fitting Parameters for $FAPbI_3$ at 20 and −130 °C

$FAPbI_3$		
description/temperature (°C)	20	−130
mobility: e^-/h^+ [$cm^2/(V{\cdot}s)$]	2.7/1.8	7.0/6.5
generation yield (k_1) [$1/cm^3/nC$]	1.65×10^{15}	1.65×10^{15}
second-order recombination rate (k_2) [cm^3/s]	3.50×10^{-9}	6.50×10^{-10}
second-order trap filling rate (k_3) [cm^3/s]	2.00×10^{-6}	3.00×10^{-7}
second-order trap emptying rate (k_4)	2.00×10^{-9}	8.00×10^{-10}
trap state concentration N_t [$1/cm^3$]	9.00×10^{14}	7.80×10^{14}

concentration of traps determined, ~8×10^{14} cm^{-3}, is in agreement to previous work under similar conditions,[5] but is substantially larger than that for single crystals (1.13×10^{10} cm^{-3}) as determined by SCLC.[25] This high concentration of traps shows that the second-order trap-filling (k_3) process is dominant here. Taking the product of the trap concentration and the second-order rate constants above results in quasi-first-order trapping rates of 1.8×10^9 s^{-1} at 20 °C and 2.3×10^8 s^{-1} at −130 °C. This rate increases with temperature pointing to charge recombination with ionized impurities.[44] The rate for second-order recombination of free electrons and holes (k_2) decreases as the temperature decreases from 3.5×10^{-9} cm^3 s^{-1} at 20 °C to 6.5×10^{-10} cm^3 s^{-1} at −130 °C. If this process would be limited by (homogeneous) charge transport, an opposite trend would be expected here: faster recombination at higher charge mobility. This shows that recombination in these materials exhibits a complicated temperature dependence in which the local dielectric environment of the charges plays an important role. Because of the disorder in the mutual orientations of the slightly dipolar formamidinium cations, a disordered energy landscape is present.[45] This disorder may result from both the electric field due to the orientation and position of the FA cation and from local distortions of the Pb-I lattice caused by this. At lower temperature, the rotational motion of the organic cation is reduced, resulting in a different, more static disorder, which may lead to the formation of separate domains for the positive and negative charges, leading to slower recombination. We have previously reported such behavior also for methylammonium-based lead perovskites,[5] however, in this case the effect was much stronger and a very abrupt change in both the charge mobility and the carrier lifetime was observed at the phase transition between tetragonal and orthorhombic phases. In the present case, due to the very small dipole moment of FA, the effect is smaller and much more gradual, however, the results do show that also in this case the orientational disorder of the organic cation plays a role in the recombination kinetics of the charges.

CONCLUSION

In this work, we have shown that the interaction of the organic cation with the structure has a large influence on the charge carrier dynamics of perovskite materials. Depending on the rotational freedom and dipole moment of the organic cation, properties such as the mobility, lifetime, and recombination rates will be affected. In $FAPbI_3$, the reduced rotational freedom of FA makes its lifetime longer than the lifetime of $MAPbI_3$. At the same time, these reduced rotational freedom and smaller dipole moment make the mobility and lifetime more independent to changes in temperature and phase transitions than for $MAPbI_3$.

ASSOCIATED CONTENT

Supporting Information

The Supporting Information is available free of charge on the ACS Publications website at DOI: 10.1021/acs.jpcc.7b09303.

XRD pattern, SEM images, DFT band structure calculations, overlapped mobility and lifetime of $MAPbI_3$ and $FAPbI_3$, and decay time constant of $FAPbI_3$ as a function of temperature (PDF)

AUTHOR INFORMATION

Corresponding Author

*E-mail: f.c.grozema@tudelft.nl. Phone: +31 6 14 38 44 41.

ORCID

Ferdinand C. Grozema: 0000-0002-4375-799X

Notes

The authors declare no competing financial interest.

ACKNOWLEDGMENTS

The research leading to these results in the Delft University of Technology has received funding from the European Research Council Horizon 2020 ERC Grant Agreement no. 648433.

REFERENCES

(1) Brenner, T. M.; Egger, D. A.; Kronik, L.; Hodes, G.; Cahen, D. Hybrid Organic—Inorganic Perovskites: Low-Cost Semiconductors with Intriguing Charge-Transport Properties. *Nat. Rev. Mater.* **2016**, *1*, 15007.

(2) Pedesseau, L.; Sapori, D.; Traore, B.; Robles, R.; Fang, H.-H.; Loi, M. A.; Tsai, H.; Nie, W.; Blancon, J.-C.; Neukirch, A.; et al. Advances and Promises of Layered Halide Hybrid Perovskite Semiconductors. *ACS Nano* **2016**, *10*, 9776−9786.

(3) Frost, J. M.; Butler, K. T.; Brivio, F.; Hendon, C. H.; van Schilfgaarde, M.; Walsh, A. Atomistic Origins of High-Performance in Hybrid Halide Perovskite Solar Cells. *Nano Lett.* **2014**, *14*, 2584−2590.

(4) Frost, J. M.; Butler, K. T.; Walsh, A. Molecular Ferroelectric Contributions to Anomalous Hysteresis in Hybrid Perovskite Solar Cells. *APL Mater.* **2014**, *2*, 081506.

(5) Gélvez-Rueda, M. C.; Cao, D. H.; Patwardhan, S.; Renaud, N.; Stoumpos, C. C.; Schatz, G. C.; Hupp, J. T.; Farha, O. K.; Savenije, T. J.; Kanatzidis, M. G.; et al. Effect of Cation Rotation on Charge Dynamics in Hybrid Lead Halide Perovskites. *J. Phys. Chem. C* **2016**, *120*, 16577−16585.

(6) Motta, C.; El-Mellouhi, F.; Kais, S.; Tabet, N.; Alharbi, F.; Sanvito, S. Revealing the Role of Organic Cations in Hybrid Halide Perovskite $CH_3NH_3PbI_3$. *Nat. Commun.* **2015**, *6*, 7026.

(7) Kamminga, M. E.; Fang, H.-H.; Filip, M. R.; Giustino, F.; Baas, J.; Blake, G. R.; Loi, M. A.; Palstra, T. T. M. Confinement Effects in Low-Dimensional Lead Iodide Perovskite Hybrids. *Chem. Mater.* **2016**, *28*, 4554−4562.

(8) Hutter, E. M.; Gelvez-Rueda, M. C.; Osherov, A.; Bulovic, V.; Grozema, F. C.; Stranks, S. D.; Savenije, T. J. Direct-Indirect Character of the Bandgap in Methylammonium Lead Iodide Perovskite. *Nat. Mater.* **2017**, *16*, 115−120.

(9) Zheng, F.; Tan, L. Z.; Liu, S.; Rappe, A. M. Rashba Spin−Orbit Coupling Enhanced Carrier Lifetime in $CH_3NH_3PbI_3$. *Nano Lett.* **2015**, *15*, 7794−7800.

(10) Stoumpos, C. C.; Malliakas, C. D.; Kanatzidis, M. G. Semiconducting Tin and Lead Iodide Perovskites with Organic Cations: Phase Transitions, High Mobilities, and near-Infrared Photoluminescent Properties. *Inorg. Chem.* **2013**, *52*, 9019−38.

(11) Hirasawa, M.; Ishihara, T.; Goto, T. Exciton Features in 0-Dimensional, 2-Dimensional, and 3-Dimensional Networks of $[PbI_6]^{4+}$ Octahedra. *J. Phys. Soc. Jpn.* **1994**, *63*, 3870−3879.

DOI: 10.1021/acs.jpcc.7b09303
J. Phys. Chem. C 2017, 121, 23392−23397

(12) Ishihara, T. Optical Properties of PbI-Based Perovskite Structures. *J. Lumin.* **1994**, *60−61*, 269−274.
(13) Papavassiliou, G. C.; Koutselas, I. B. Structural, Optical and Related Properties of Some Natural Three- and Lower-Dimensional Semiconductor Systems. *Synth. Met.* **1995**, *71*, 1713−1714.
(14) Stoumpos, C. C.; Cao, D. H.; Clark, D. J.; Young, J.; Rondinelli, J. M.; Jang, J. I.; Hupp, J. T.; Kanatzidis, M. G. Ruddlesden−Popper Hybrid Lead Iodide Perovskite 2d Homologous Semiconductors. *Chem. Mater.* **2016**, *28*, 2852−2867.
(15) Eperon, G. E.; Stranks, S. D.; Menelaou, C.; Johnston, M. B.; Herz, L. M.; Snaith, H. J. Formamidinium Lead Trihalide: A Broadly Tunable Perovskite for Efficient Planar Heterojunction Solar Cells. *Energy Environ. Sci.* **2014**, *7*, 982−988.
(16) Koh, T. M.; Fu, K. W.; Fang, Y. N.; Chen, S.; Sum, T. C.; Mathews, N.; Mhaisalkar, S. G.; Boix, P. P.; Baikie, T. Formamidinium-Containing Metal-Halide: An Alternative Material for near-Ir Absorption Perovskite Solar Cells. *J. Phys. Chem. C* **2014**, *118*, 16458−16462.
(17) Lee, J. W.; Seol, D. J.; Cho, A. N.; Park, N. G. High-Efficiency Perovskite Solar Cells Based on the Black Polymorph of $HC(NH_2)_2PbI_3$. *Adv. Mater.* **2014**, *26*, 4991−4998.
(18) Lv, S. L.; Pang, S. P.; Zhou, Y. Y.; Padture, N. P.; Hu, H.; Wang, L.; Zhou, X. H.; Zhu, H. M.; Zhang, L. X.; Huang, C. S.; et al. One-Step, Solution-Processed Formamidinium Lead Trihalide ($FAPbI_{(3-x)}Cl_x$) for Mesoscopic Perovskite-Polymer Solar Cells. *Phys. Chem. Chem. Phys.* **2014**, *16*, 19206−19211.
(19) Hanusch, F. C.; Wiesenmayer, E.; Mankel, E.; Binek, A.; Angloher, P.; Fraunhofer, C.; Giesbrecht, N.; Feckl, J. M.; Jaegermann, W.; Johrendt, D.; et al. Efficient Planar Heterojunction Perovskite Solar Cells Based on Formamidinium Lead Bromide. *J. Phys. Chem. Lett.* **2014**, *5*, 2791−2795.
(20) Pellet, N.; Gao, P.; Gregori, G.; Yang, T.-Y.; Nazeeruddin, M. K.; Maier, J.; Grätzel, M. Mixed-Organic-Cation Perovskite Photovoltaics for Enhanced Solar-Light Harvesting. *Angew. Chem., Int. Ed.* **2014**, *53*, 3151−3157.
(21) Pang, S.; Hu, H.; Zhang, J.; Lv, S.; Yu, Y.; Wei, F.; Qin, T.; Xu, H.; Liu, Z.; Cui, G. $NH_2CH{=}NH_2PbI_3$: An Alternative Organolead Iodide Perovskite Sensitizer for Mesoscopic Solar Cells. *Chem. Mater.* **2014**, *26*, 1485−1491.
(22) Binek, A.; Hanusch, F. C.; Docampo, P.; Bein, T. Stabilization of the Trigonal High-Temperature Phase of Formamidinium Lead Iodide. *J. Phys. Chem. Lett.* **2015**, *6*, 1249−1253.
(23) Han, Q.; Bae, S.-H.; Sun, P.; Hsieh, Y.-T.; Yang, Y.; Rim, Y. S.; Zhao, H.; Chen, Q.; Shi, W.; Li, G.; et al. Single Crystal Formamidinium Lead Iodide ($FAPbI_3$): Insight into the Structural, Optical, and Electrical Properties. *Adv. Mater.* **2016**, *28*, 2253−2258.
(24) Fang, H.-H.; Wang, F.; Adjokatse, S.; Zhao, N.; Even, J.; Antonietta Loi, M. Photoexcitation Dynamics in Solution-Processed Formamidinium Lead Iodide Perovskite Thin Films for Solar Cell Applications. *Light: Sci. Appl.* **2016**, *5*, e16056.
(25) Zhumekenov, A. A.; Saidaminov, M. I.; Haque, M. A.; Alarousu, E.; Sarmah, S. P.; Murali, B.; Dursun, I.; Miao, X.-H.; Abdelhady, A. L.; Wu, T.; et al. Formamidinium Lead Halide Perovskite Crystals with Unprecedented Long Carrier Dynamics and Diffusion Length. *ACS Energy Lett.* **2016**, *1*, 32−37.
(26) Wright, A. D.; Verdi, C.; Milot, R. L.; Eperon, G. E.; Pérez-Osorio, M. A.; Snaith, H. J.; Giustino, F.; Johnston, M. B.; Herz, L. M. Electron−Phonon Coupling in Hybrid Lead Halide Perovskites. *Nat. Commun.* **2016**, *7*, 11755.
(27) Bakulin, A. A.; Selig, O.; Bakker, H. J.; Rezus, Y. L. A.; Muller, C.; Glaser, T.; Lovrincic, R.; Sun, Z. H.; Chen, Z. Y.; Walsh, A.; et al. Real-Time Observation of Organic Cation Reorientation in Methylammonium Lead Iodide Perovskites. *J. Phys. Chem. Lett.* **2015**, *6*, 3663−3669.
(28) Weller, M. T.; Weber, O. J.; Frost, J. M.; Walsh, A. Cubic Perovskite Structure of Black Formamidinium Lead Iodide, α-$[HC(NH_2)_2]PbI_3$, at 298 K. *J. Phys. Chem. Lett.* **2015**, *6*, 3209−3212.
(29) Onodayamamuro, N.; Matsuo, T.; Suga, H. Dielectric Study of CH_3NH_3PbX3 (X = Cl, Br, I). *J. Phys. Chem. Solids* **1992**, *53*, 935−939.
(30) Fabini, D. H.; Hogan, T.; Evans, H. A.; Stoumpos, C. C.; Kanatzidis, M. G.; Seshadri, R. Dielectric and Thermodynamic Signatures of Low-Temperature Glassy Dynamics in the Hybrid Perovskites $CH_3NH_3PbI_3$ and $HC(NH_2)_2PbI_3$. *J. Phys. Chem. Lett.* **2016**, *7*, 376−381.
(31) Fabini, D. H.; Stoumpos, C. C.; Laurita, G.; Kaltzoglou, A.; Kontos, A. G.; Falaras, P.; Kanatzidis, M. G.; Seshadri, R. Reentrant Structural and Optical Properties and Large Positive Thermal Expansion in Perovskite Formamidinium Lead Iodide. *Angew. Chem., Int. Ed.* **2016**, *55*, 15392−15396.
(32) Warman, J. M.; Gelinck, G. H.; de Haas, M. P. The Mobility and Relaxation Kinetics of Charge Carriers in Molecular Materials Studied by Means of Pulse-Radiolysis Time-Resolved Microwave Conductivity: Dialkoxy-Substituted Phenylene-Vinylene Polymers. *J. Phys.: Condens. Matter* **2002**, *14*, 9935−9954.
(33) Warman, J. M.; de Haas, M. P.; Dicker, G.; Grozema, F. C.; Piris, J.; Debije, M. G. Charge Mobilities in Organic Semiconducting Materials Determined by Pulse-Radiolysis Time-Resolved Microwave Conductivity: π-Bond-Conjugated Polymers Versus π-π-Stacked Discotics. *Chem. Mater.* **2004**, *16*, 4600−4609.
(34) Grozema, F. C. Opto-Electronic Properties of Conjugated Molecular Wires. Doctoral Thesis, Delft University of Technology, Delft, The Netherlands, 2003.
(35) Herz, L. M. Charge-Carrier Mobilities in Metal Halide Perovskites: Fundamental Mechanisms and Limits. *ACS Energy Lett.* **2017**, *2*, 1539−1548.
(36) Neamen, D. A. *Semiconductor Physics and Devices: Basic Principles*; McGraw-Hill: London, 2012.
(37) Yu, P. Y.; Cardona, M. *Fundamentals of Semiconductors: Physics and Materials Properties*; Springer: Berlin, 2005.
(38) Li, B.; Kawakita, Y.; Liu, Y. C.; Wang, M. C.; Matsuura, M.; Shibata, K.; Ohira-Kawamura, S.; Yamada, T.; Lin, S. C.; Nakajima, K. J.; et al. Polar Rotor Scattering as Atomic-Level Origin of Low Mobility and Thermal Conductivity of Perovskite Ch3nh3pbi3. *Nat. Commun.* **2017**, *8*, 16086.
(39) Swainson, I. P.; Stock, C.; Parker, S. F.; Van Eijck, L.; Russina, M.; Taylor, J. W. From Soft Harmonic Phonons to Fast Relaxational Dynamics in $CH_3NH_3PbBr_3$. *Phys. Rev. B: Condens. Matter Mater. Phys.* **2015**, *92*, 100303.
(40) Knop, O.; Wasylishen, R. E.; White, M. A.; Cameron, T. S.; Van Oort, M. J. M. Alkylammonium Lead Halides. Part 2. $CH_3NH_3PbX_3$ (X = Cl, Br, I) Perovskites - Cuboctahedral Halide Cages with Isotropic Cation Reorientation. *Can. J. Chem.* **1990**, *68*, 412−422.
(41) Jiang, C. S.; Yang, M. J.; Zhou, Y. Y.; To, B.; Nanayakkara, S. U.; Luther, J. M.; Zhou, W. L.; Berry, J. J.; van de Lagemaat, J.; Padture, N. P.; et al. Carrier Separation and Transport in Perovskite Solar Cells Studied by Nanometre-Scale Profiling of Electrical Potential. *Nat. Commun.* **2015**, *6*, 8397.
(42) Green, M. A.; Emery, K.; Hishikawa, Y.; Warta, W.; Dunlop, E. D. Solar Cell Efficiency Tables (Version 46). *Prog. Photovoltaics* **2015**, *23*, 805−812.
(43) Hutter, E. M.; Eperon, G. E.; Stranks, S. D.; Savenije, T. J. Charge Carriers in Planar and Meso-Structured Organic-Inorganic Perovskites: Mobilities, Lifetimes, and Concentrations of Trap States. *J. Phys. Chem. Lett.* **2015**, *6*, 3082−3090.
(44) Milot, R. L.; Eperon, G. E.; Snaith, H. J.; Johnston, M. B.; Herz, L. M. Temperature-Dependent Charge-Carrier Dynamics in $CH_3NH_3PbI_3$ Perovskite Thin Films. *Adv. Funct. Mater.* **2015**, *25*, 6218−6227.
(45) Hilczer, M.; Tachiya, M. Unified Theory of Geminate and Bulk Electron-Hole Recombination in Organic Solar Cells. *J. Phys. Chem. C* **2010**, *114*, 6808−6813.

DOI: 10.1021/acs.jpcc.7b09303
J. Phys. Chem. C 2017, 121, 23392−23397